



Title	Effect of Strain on Room-Temperature Spin Transport in $\text{Si}_{0.1}\text{Ge}_{0.9}$
Author(s)	Naito, T.; Yamada, M.; Wagatsuma, Y. et al.
Citation	Physical Review Applied. 2022, 18(2), p. 024005
Version Type	VoR
URL	https://hdl.handle.net/11094/89427
rights	Copyright 2022 by the American Physical Society
Note	

The University of Osaka Institutional Knowledge Archive : OUKA

<https://ir.library.osaka-u.ac.jp/>

The University of Osaka

Effect of Strain on Room-Temperature Spin Transport in $\text{Si}_{0.1}\text{Ge}_{0.9}$

T. Naito,¹ M. Yamada,^{2,3} Y. Wagatsuma,⁴ K. Sawano,⁴ and K. Hamaya^{1,3,5,*}


¹*Department of Systems Innovation, Graduate School of Engineering Science, Osaka University, 1-3 Machikaneyama, Toyonaka 560-8531, Japan*

²*PRESTO, Japan Science and Technology Agency, 4-1-8 Honcho, Kawaguchi, Saitama 332-0012, Japan*

³*Center for Spintronics Research Network, Graduate School of Engineering Science, Osaka University, 1-3 Machikaneyama, Toyonaka 560-8531, Japan*

⁴*Advanced Research Laboratories, Tokyo City University, 8-15-1 Todoroki, Tokyo 158-0082, Japan*

⁵*Spintronics Research Network Division, Institute for Open and Transdisciplinary Research Initiatives, Osaka University, Yamadaoka 2-1, Suita, Osaka 565-0871, Japan*

 (Received 18 October 2021; revised 25 May 2022; accepted 8 June 2022; published 2 August 2022)

We report a strain effect on spin transport in semiconductors that exhibit Ge-like conduction bands at room temperature. Using four-terminal nonlocal spin-transport measurements in lateral spin-valve devices, we experimentally estimate the spin diffusion length (λ) of Ge and strained $\text{Si}_{0.1}\text{Ge}_{0.9}$ with two different carrier concentrations. Despite the Ge-like electronic band structure, the obtained λ of a strained $\text{Si}_{0.1}\text{Ge}_{0.9}$ is comparable to that of a Si channel. We discuss a possible mechanism of the strain-induced enhancement of λ at room temperature. As a consequence, we demonstrate the electrical detection of 5- μm lateral spin transport in the strained $\text{Si}_{0.1}\text{Ge}_{0.9}$ by applying an electric field at room temperature.

DOI: [10.1103/PhysRevApplied.18.024005](https://doi.org/10.1103/PhysRevApplied.18.024005)

I. INTRODUCTION

Lattice strain in semiconductors enables modification of their electronic band structure, including their band gap, electronic charge density, and phonon frequency [1–6]. In particular, strained III-V and group-IV semiconductors have been widely investigated theoretically and experimentally because lattice strain can be applied in these materials through heterointerfaces formed via epitaxial growth techniques, leading to advances in the field of condensed-matter physics and to various applications [7–14]. Recent studies of two-dimensional semiconductors have revealed an alternative strain effect on the electronic band structures and band gaps even in graphene [15,16], transition-metal dichalcogenides [17,18], and monolayer honeycomb elements [19–21].

Thus far, electron and hole mobility have been enhanced by in-plane biaxial or longitudinal uniaxial strain in group-IV channel layers [7–11]. For example in Ge(111), the in-plane biaxial and tensile strain causes energy splitting between a onefold and threefold L valley in the conduction band, leading to electrons occupying a onefold L valley with greater electron mobility [22–24]. In addition, the lattice strain in Ge induced by Si dramatically changes the physical properties because of the energy proximity

(approximately 140 meV) between the conduction-band minima at L points and the Γ point. Tensile strain is well known to decrease the energy difference between the L and Γ gaps, enhancing the optically accessible nature of Ge [25,26]. Even for spins, Bottegoni *et al.* and Pezzoli *et al.* have reported on the high spin polarization and long spin lifetime in strained Ge layers or Ge quantum wells grown on SiGe [27–30], respectively, lifting the heavy-hole–light-hole degeneracy in the valence band of Ge. Recently, Cesari *et al.* [31] used strained Ge-rich $\text{Ge}_{1-x}\text{Sn}_x$ alloys to effectively explore spin-related optical properties.

Theoretical and experimental studies on the effect of strain on the spin-relaxation mechanism in Si and/or Ge have also been reported. In particular, because the dominant spin relaxation pathway in Si and Ge is spin-flip scattering between the conduction-band valleys (i.e., intervalley spin-flip scattering) induced by electron-phonon [32–38] and electron-impurity interactions [39–41] through the spin-orbit coupling in host materials and impurities, respectively. Tang *et al.*, Li *et al.*, and Chalaev *et al.* have theoretically predicted suppression of intervalley spin-flip scattering through the strain, leading to lifting of the degenerate valleys at six Δ points for Si or at four L points for Ge [33,35,42]. Even in the case of pure spin-current transport, the impurity-induced intervalley spin-flip scattering was partly suppressed at low temperatures

*hamaya.kohei.es@osaka-u.ac.jp

when a strained heavily doped n -Si_{0.1}Ge_{0.9}(111) layer was used [43], where the Ge-rich Si_{1-x}Ge_x exhibited a Ge-like electronic band structure with conduction-band minima at L points. However, because of the marked influences of electron-phonon interactions and experimental difficulties, it has been difficult to clarify the effect of the lattice strain on the spin transport in group-IV semiconductors at room temperature.

Here we report a strain-induced enhancement in one of the spin-related physical properties, the spin-diffusion length (λ), in a semiconductor at room temperature. Note that the difference in the band structure between Si_{0.1}Ge_{0.9} and pure Ge is quite small [44,45] and the position of the Fermi level (E_F) can easily be tuned by varying the doping concentration in the Si_{0.1}Ge_{0.9} and pure Ge channel. Using four-terminal nonlocal spin-transport measurements in lateral spin-valve (LSV) devices, we clearly observe room-temperature spin transport in the strained Si_{0.1}Ge_{0.9} and experimentally estimate the λ of the strained Si_{0.1}Ge_{0.9}. As a consequence, for an electron carrier concentration (n) of $1 \times 10^{18} \text{ cm}^{-3}$, the λ of the strained Si_{0.1}Ge_{0.9} is much larger than that of the pure Ge. Despite the Ge-like electronic band structure, the obtained λ of the strained Si_{0.1}Ge_{0.9} is comparable to that of a Si channel at room temperature in Ref. [40]. We discuss a possible origin of the strain-induced enhancement of λ and demonstrate the electrical detection of 5- μm lateral spin transport in the strained Si_{0.1}Ge_{0.9} by applying an electric field at room temperature.

II. RESULTS AND DISCUSSION

A. Growth and electrical properties of strained Si_{0.1}Ge_{0.9}

We prepare coherently grown Ge-rich Si_{1-x}Ge_x (Si_{0.1}Ge_{0.9}) and Ge spin-transport layers on a Ge buffer layer on Si(111) substrate. Figure 1(a) shows a schematic and the nominal thicknesses of the n -Si_{0.1}Ge_{0.9} spin-transport layer grown on a Ge buffer layer/Si(111). Here, the heterostructure is grown by molecular beam epitaxy (MBE) as follows. First, a Ge(111) buffer layer on an undoped Si(111) substrate ($\rho \sim 1000 \text{ } \Omega \text{ cm}$) is formed via a two-step growth method [46], where the first undoped Ge layer (approximately 30 nm) is grown at 350 °C (LT-Ge), followed by an undoped Ge layer (approximately 500 nm) grown at 700 °C (HT-Ge). The Ge buffer layer is relaxed, and misfit dislocations are confined near the Ge/Si(111) interface, as shown in Ref. [43]. On top of the HT-Ge layer, a 70-nm-thick phosphorus (P)-doped n -Si_{0.1}Ge_{0.9}(111) layer is grown by MBE at 350 °C [47]. Finally, a 7-nm-thick P δ -doped Ge layer with a 0.3-nm-thick Si layer is grown on top of the spin-transport layer for the Schottky tunnel conduction of electrons in spin-transport measurements [48]. As a reference, 140-nm-thick P-doped n -Ge(111) layers on a HT-Ge layer

(approximately 70 nm) [49] are also prepared to verify the strain effect. Figure 1(b) displays a two-dimensional x-ray diffraction (XRD) reciprocal space map for the grown Si_{0.1}Ge_{0.9}/Ge/Si(111) heterostructure, where Q_x and Q_z are the reciprocal space lattice parameters for in-plane and out-of-plane, respectively. Because of the difference in the lattice constant between Si and Ge, the (Q_x, Q_z) positions between the Si substrate and the grown Ge buffer layer differ dramatically. However, we observe matching of the Q_x parameter between the Ge buffer layer and the grown Si_{0.1}Ge_{0.9} layer. This matching means that the grown Si_{0.1}Ge_{0.9} layer on the Ge buffer layer is fully strained toward the layer plane, indicating biaxial tensile strain (ϵ_x) in (111). A comparison of the lattice constant of the strained Si_{0.1}Ge_{0.9} and that reported for unstrained Si_{0.1}Ge_{0.9} [50] indicates that the value of ϵ_x should be 0.64%–0.66%. Here we should also consider the presence of the tensile strain ($\epsilon_x \sim 0.2\%$) in the Ge buffer layer from the Si substrate due to the mismatch in thermal expansion coefficients between Ge and Si. However, there was no impact on the electron Hall mobility and spin-diffusion length at room temperature for the Ge spin-transport layers studied in the present study. Thus, in the strained Si_{0.1}Ge_{0.9}, we can simply predict that the four degenerate L valleys are lifted into a onefold low-energy valley and threefold higher-energy valleys [22–24,33,35], as depicted in the inset of Fig. 1(c).

To measure the electrical properties of the strained Si_{0.1}Ge_{0.9} layer, we process the heterostructure into Hall bar devices. From the longitudinal resistance (V_{xx}/I) and Hall voltage (V_{xy}) measurements, we determine the electrical resistivity (ρ) and electron carrier concentration (n) and estimated the electron mobility (μ) [Fig. 1(c)] at room temperature for the strained Si_{0.1}Ge_{0.9} and Ge layers. By tuning the doping concentration of P in the channel layers, we prepared Ge and strained Si_{0.1}Ge_{0.9} layers with two different n values: approximately $5 \times 10^{18} \text{ cm}^{-3}$ and approximately $1 \times 10^{18} \text{ cm}^{-3}$ [bottom of Fig. 1(c)]. Thus, in the present study, we compare these four channels to clarify the strain effect on room-temperature spin transport in semiconductors. Here the HT-Ge layer is undoped but exhibits p -type conduction due to the defect-induced hole generation [46], leading to the formation of a p - n junction at the n -SiGe/HT-Ge heterointerface [Fig. 1(d)]. As a result, the electron spin diffusion toward the Ge-on-Si substrate can be suppressed. Of note, the strained Si_{0.1}Ge_{0.9} layer with $n \sim 1 \times 10^{18} \text{ cm}^{-3}$ clearly shows an almost twofold enhancement in μ at room temperature. This enhancement is consistent with the increase in the population of conduction electrons in the lowest L valley, which has a relatively small electron effective mass compared with the other three valleys [22–24]. On the basis of the literature [51,52], the energy splitting of the conduction L valleys for the strained Si_{0.1}Ge_{0.9} is theoretically expected to be 55–90 meV.

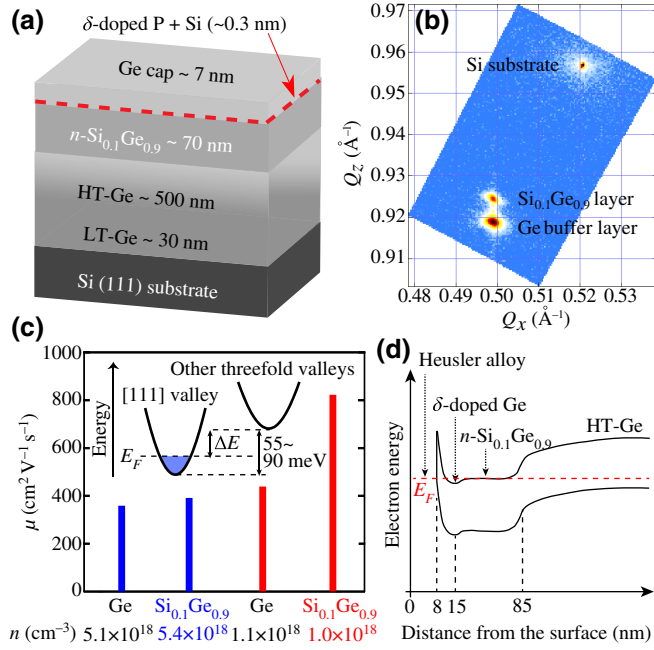


FIG. 1. (a) Schematic of the grown $n\text{-Si}_{0.1}\text{Ge}_{0.9}/\text{Ge}/\text{Si}(111)$ heterostructure for spin-transport measurements of the strained $n\text{-Si}_{0.1}\text{Ge}_{0.9}$. (b) Asymmetric (153) reciprocal space map of the $\text{Si}_{0.1}\text{Ge}_{0.9}/\text{Ge}/\text{Si}(111)$. The $\text{Si}_{0.1}\text{Ge}_{0.9}$ layer is fully strained on the Ge buffer layer. (c) Electron Hall mobility of the strained $n\text{-Si}_{0.1}\text{Ge}_{0.9}$ and $n\text{-Ge}$ with relatively high (approximately $5 \times 10^{18} \text{ cm}^{-3}$) and low (approximately $1 \times 10^{18} \text{ cm}^{-3}$) carrier concentrations at 300 K. The inset shows a schematic of the conduction-band valleys in the strained $n\text{-Si}_{0.1}\text{Ge}_{0.9}$. (d) Schematic of a band lineup of a part of the Co-based Heusler/P δ -doped Ge/ $n\text{-Si}_{0.1}\text{Ge}_{0.9}$ /HT-Ge (p -Ge).

B. Spin transport in strained $\text{Si}_{0.1}\text{Ge}_{0.9}$

To examine the spin transport in semiconductors, we focus on four-terminal nonlocal voltage measurements in LSV devices [53,54]. The top view of a fabricated LSV device with the strained $n\text{-Si}_{0.1}\text{Ge}_{0.9}$ channel layer is shown in Fig. 2(a), where d is the edge-to-edge distance between the spin injector and the detector. The size of the spin injector (detector) contact is $0.4 \times 5.0 \mu\text{m}^2$ ($1.0 \times 5.0 \mu\text{m}^2$). Details of the fabrication processes and top views of similar LSV devices have been reported elsewhere [48,55]. As the spin injector and detector materials, we use Co-based Heusler alloys [56,57] such as $\text{Co}_2\text{FeAl}_{0.5}\text{Si}_{0.5}$ and Co_2MnSi , which are grown by MBE on top of the Schottky tunnel barriers [48,58]. Here, a 0.7-nm-thick Fe layer is inserted between the Co-based Heusler alloy and the Ge cap layer to obtain large spin signals at room temperature [59,60]. All the measurements are carried out at room temperature (approximately 298 K) by applying a negative direct current ($I < 0$), for which the spin-polarized electrons are injected into the

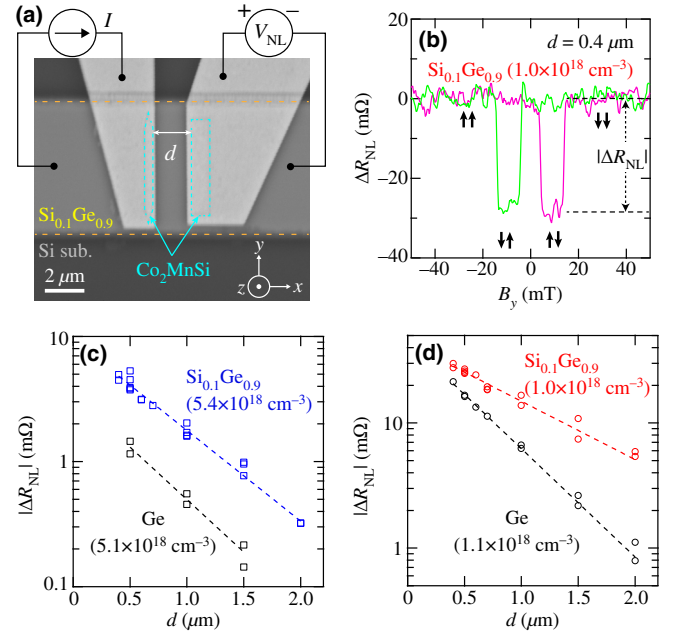


FIG. 2. (a) SEM image of a lateral spin-valve (LSV) device fabricated using the strained $n\text{-Si}_{0.1}\text{Ge}_{0.9}$. (b) A nonlocal spin signal $[\Delta R_{\text{NL}} = \Delta V_{\text{NL}}/I = (V_{\text{NL}}^{\downarrow\downarrow} - V_{\text{NL}}^{\uparrow\uparrow})/I]$ as a function of B_y for a LSV device ($d = 0.4 \mu\text{m}$) with the strained $n\text{-Si}_{0.1}\text{Ge}_{0.9}$ with $n \sim 1.0 \times 10^{18} \text{ cm}^{-3}$. Hysteretic behavior depending on the magnetization switching between the parallel and antiparallel states is clearly observed at room temperature. Here, the magnitude of ΔR_{NL} , $|\Delta R_{\text{NL}}|$, can be determined as described in Fig. 2(b). To estimate λ , we plot $|\Delta R_{\text{NL}}|$ as a function of d for the strained $\text{Si}_{0.1}\text{Ge}_{0.9}$ and Ge LSV devices with $n \sim 5 \times 10^{18} \text{ cm}^{-3}$ and $n \sim 1 \times 10^{18} \text{ cm}^{-3}$ in Figs. 2(c) and 2(d), respectively. For all the four-channel LSV devices, $|\Delta R_{\text{NL}}|$ is found to decay exponentially with increasing d .

semiconductor channel used here, under applied in-plane (B_y) or out-of-plane (B_z) magnetic fields.

Figure 2(b) shows a representative nonlocal spin signal $[\Delta R_{\text{NL}} = \Delta V_{\text{NL}}/I = (V_{\text{NL}}^{\downarrow\downarrow} - V_{\text{NL}}^{\uparrow\uparrow})/I]$ as a function of B_y for a LSV device ($d = 0.4 \mu\text{m}$) with the strained $n\text{-Si}_{0.1}\text{Ge}_{0.9}$ with $n \sim 1.0 \times 10^{18} \text{ cm}^{-3}$. Hysteretic behavior depending on the magnetization switching between the parallel and antiparallel states is clearly observed at room temperature. Here, the magnitude of ΔR_{NL} , $|\Delta R_{\text{NL}}|$, can be determined as described in Fig. 2(b). To estimate λ , we plot $|\Delta R_{\text{NL}}|$ as a function of d for the strained $\text{Si}_{0.1}\text{Ge}_{0.9}$ and Ge LSV devices with $n \sim 5 \times 10^{18} \text{ cm}^{-3}$ and $n \sim 1 \times 10^{18} \text{ cm}^{-3}$ in Figs. 2(c) and 2(d), respectively. For all the four-channel LSV devices, $|\Delta R_{\text{NL}}|$ is found to decay exponentially with increasing d .

In general, the reduction in $|\Delta R_{\text{NL}}|$ with increasing d can be represented by the following equation [48,53,54]:

$$|\Delta R_{\text{NL}}| = P^2 \frac{\rho \lambda}{S} \exp(-d/\lambda), \quad (1)$$

where P is the average of the spin injection and detection efficiency and S is the cross-section area of the semiconductor channels (approximately $0.49 \mu\text{m}^2$ for $n\text{-Si}_{0.1}\text{Ge}_{0.9}$ and approximately $0.98 \mu\text{m}^2$ for $n\text{-Ge}$). Here, we use the estimated ρ values of 7.5 and

TABLE I. Spin-diffusion length (λ), diffusion constant (D), and spin lifetime (τ) at room temperature for various semiconductor channels.

Channel	n (cm $^{-3}$)	λ (μ m)	D (cm 2 /s)	τ (ns)
Si $_{0.1}$ Ge $_{0.9}$	1.0×10^{18}	0.93	32	0.27
Ge	1.1×10^{18}	0.50	17	0.15
Si $_{0.1}$ Ge $_{0.9}$	5.4×10^{18}	0.60	23	0.16
Ge	5.1×10^{18}	0.52	21	0.13
Si [40]	1.6×10^{19}	0.95	4.4	2.1

3.0 m Ω cm for the strained n -Si $_{0.1}$ Ge $_{0.9}$ with $n \sim 1.0 \times 10^{18}$ cm $^{-3}$ and $\sim 5.4 \times 10^{18}$ cm $^{-3}$, respectively; by contrast, for the Ge with $n \sim 1.1 \times 10^{18}$ cm $^{-3}$ and $\sim 5.1 \times 10^{18}$ cm $^{-3}$, we use the ρ values of 13.3 and 3.4 m Ω cm, respectively. As shown by the dashed curves in Figs. 2(c) and 2(d), all the decay behaviors can be fitted using Eq. (1), leading to the estimate of λ . Notably, the slope of the dashed curves for the strained n -Si $_{0.1}$ Ge $_{0.9}$ is smaller than that for the Ge in both Figs. 2(c) and 2(d).

Table I shows a summary of the estimated λ values at room temperature for all four channels, together with the value for heavily doped Si [40]. The largest λ of 0.93 μ m is obtained for the strained Si $_{0.1}$ Ge $_{0.9}$ with $n \sim 1 \times 10^{18}$ cm $^{-3}$. Notably, the λ of 0.93 μ m is large compared with that for the Ge ($n \sim 1 \times 10^{18}$ cm $^{-3}$). In addition, even for the SiGe channel with a Ge-like electronic band structure, the value of 0.93 μ m for the strained Si $_{0.1}$ Ge $_{0.9}$ is comparable to that (approximately 0.95 μ m [40]) for a Si channel with $n \sim 1.6 \times 10^{19}$ cm $^{-3}$. This means that the lattice strain enhances the electron spin-diffusion length in a semiconductor channel.

To elucidate the mechanism of the marked enhancement in λ in the strained n -Si $_{0.1}$ Ge $_{0.9}$ even at room temperature, we further estimate the spin lifetime (τ) using the relation $\lambda = \sqrt{D\tau}$, where D is the diffusion constant. In the present study, the value of D is determined from the modified Einstein's relation in Eq. (4) in Ref. [61] and the experimentally obtained n and μ in Fig. 1(c). The largest D of approximately 32 cm 2 /s is obtained for the strained n -Si $_{0.1}$ Ge $_{0.9}$ with $n \sim 1 \times 10^{18}$ cm $^{-3}$, which is already expected from its largest electron mobility in Fig. 1(c). In addition to the D , the calculated τ for all four channels are also shown in Table I. The longest τ of approximately 0.27 ns is also obtained for the strained n -Si $_{0.1}$ Ge $_{0.9}$ with $n \sim 1 \times 10^{18}$ cm $^{-3}$. This feature indicates that suppression of an electron spin relaxation becomes evident in the strained n -Si $_{0.1}$ Ge $_{0.9}$ with $n \sim 1 \times 10^{18}$ cm $^{-3}$. From the above, we conclude the enhancement in λ attributes not only to the enhancement in D but to the enhancement in τ . We also find almost no difference in τ between the Ge with $n \sim 1 \times 10^{18}$ cm $^{-3}$ and that with $n \sim 5 \times 10^{18}$ cm $^{-3}$. Thus, for Ge at room temperature, the phonon-induced

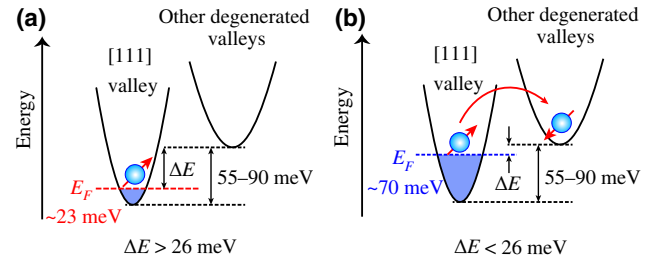


FIG. 3. Schematics of the conduction-band valleys in the strained n -Si $_{0.1}$ Ge $_{0.9}$ with (a) $n \sim 1 \times 10^{18}$ cm $^{-3}$ and (b) $n \sim 5 \times 10^{18}$ cm $^{-3}$ at room temperature.

spin relaxation is dominant rather than the donor-driven spin relaxation [43].

A simple picture of the suppression mechanism of spin relaxation is drawn in Fig. 3. Here the E_F above the conduction-band edge is roughly estimated as $\hbar^2(3\pi^2n)^{2/3}/(2m_e)$ and the valley energy splitting (55–90 meV) after applying a biaxial tensile strain in (111) to a Ge-like conduction band is also shown by referring to the literature [51,52]. Figures 3(a) and 3(b) show schematics of the correlation between the valley energy splitting and E_F for the strained n -Si $_{0.1}$ Ge $_{0.9}$ with $n \sim 1 \times 10^{18}$ cm $^{-3}$ and $n \sim 5 \times 10^{18}$ cm $^{-3}$, respectively. In both cases, we concentrate on the energy difference (ΔE) between the valley energy splitting and E_F . When the ΔE is greater than approximately 26 meV (300 K), the phonon-induced spin-flip scattering between valleys can be suppressed even at room temperature [Fig. 3(a)]. On the other hand, if the ΔE becomes less than approximately 26 meV, phonon-induced intervalley scattering can occur frequently [Fig. 3(b)]. Thus, in addition to the formation of the valley energy splitting, the position of the E_F should be considered when a semiconductor channel is designed as a room-temperature spin-transport layer.

C. Spin drift in strained Si $_{0.1}$ Ge $_{0.9}$

Until now, long-distance spin transport in semiconductors such as Si [62–65] and Ge [37] has been electrically detected by a method using a spin-drift effect. However, for Ge-like conduction-band channels, no study of the electrical detection of the long-distance spin transport at room temperature has been reported. Thus, we here explore the effect of strain on the long-distance spin transport in LSV devices at room temperature. For the strained n -Si $_{0.1}$ Ge $_{0.9}$ with $n \sim 1.0 \times 10^{18}$ cm $^{-3}$, we measure three-terminal nonlocal spin signals detected in the terminal configuration depicted in Fig. 4(a), where a negative direct current ($I_D < 0$) is applied between the spin injector and the detector contacts [64,66]. Figure 4(b) shows the room-temperature three-terminal nonlocal spin signal [$\Delta R_{3T} = \Delta V_{3T}/I_D = (V_{3T}^{\uparrow\downarrow} - V_{3T}^{\uparrow\uparrow})/I_D$] as a function of B_y at $d = 5$ μ m and at $I_D = -1$ mA. Despite the Ge-like conduction channel, a

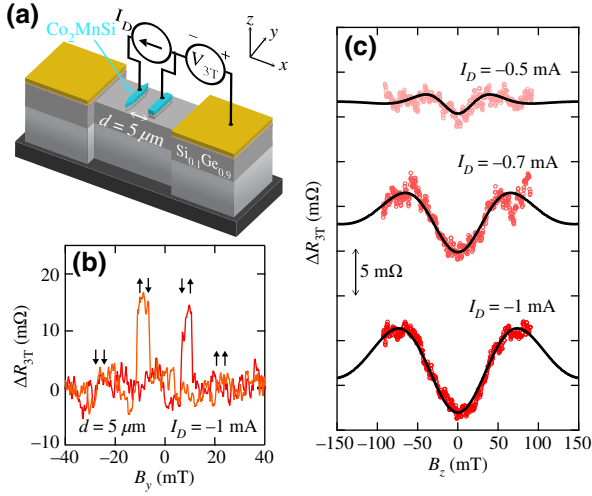


FIG. 4. (a) Schematic of a LSV device fabricated using the strained n -Si_{0.1}Ge_{0.9} ($n \sim 1.0 \times 10^{18} \text{ cm}^{-3}$) for three-terminal nonlocal spin-transport measurements. (b) Three-terminal nonlocal spin signal at $d = 5 \mu\text{m}$, at $I_D = -1 \text{ mA}$, and at room temperature. (c) Hanle precession signals in a parallel magnetization state at $d = 5 \mu\text{m}$, at various I_D of -0.5 , -0.7 , and -1 mA , and at room temperature. The solid curves are curves simulated using Eq. (2).

lateral spin transport of $5 \mu\text{m}$ is electrically detected in a LSV device with the strained Si_{0.1}Ge_{0.9} at room temperature unlike its optical detection [67,68]. By applying out-of-plane magnetic fields (B_z), we also observe Hanle precession signals in a parallel magnetization state at various I_D in Fig. 4(c). The solid curves are simulated curves based on the following equation [53,54]:

$$\Delta R(B_z) = \pm \frac{P^2 \rho D}{S} \int_0^\infty \frac{1}{\sqrt{4\pi Dt}} \exp\left[-\frac{(l - v_d t)^2}{4Dt}\right] \times \cos\left(\frac{g\mu_B B_z}{\hbar} t\right) \exp\left(-\frac{t}{\tau}\right) dt, \quad (2)$$

where $D = 32 \text{ cm}^2/\text{s}$ and $\tau = 0.27 \text{ ns}$ are fixed to the values in Table I, the center-to-center distance (l) between the spin injector and detector contacts is $5.45 \mu\text{m}$ (corresponding to the edge-to-edge distance d of $5 \mu\text{m}$), $\rho = 7.5 \text{ m}\Omega \text{ cm}$, and the drift velocity (v_d) is the product of the mobility $\mu = 823 \text{ cm}^2 \text{ V}^{-1} \text{ s}^{-1}$ in Fig. 1(c). The electron g factor (g) is set as a free parameter and is roughly estimated to be 1.13 – 1.47 , which falls in the range from 0.82 (electrons populate only in the lower energy L valley) to 1.56 (electrons populate equally in the four L valleys) [52]. When the values of P , which only affect the amplitude of the Hanle curves, are selected to be 1.61 , 2.38 , and 2.55% for $I_D = -0.5$, -0.7 , and -1 mA , respectively, the simulated curves show good agreement with the experimental results. Notably, the difference in the P values among various I_D originates mainly from an enhancement

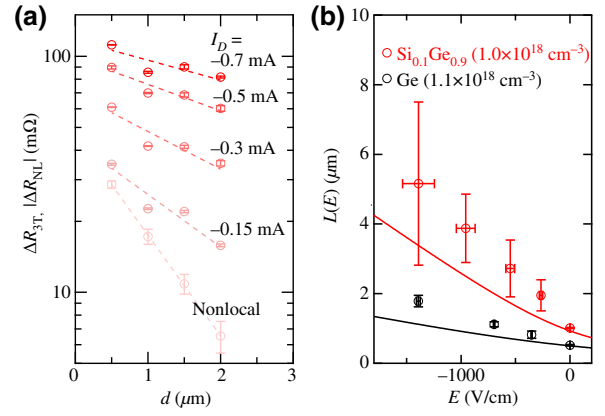


FIG. 5. (a) d dependence of ΔR_{3T} at room temperature for the strained Si_{0.1}Ge_{0.9} with $n \sim 1 \times 10^{18} \text{ cm}^{-3}$, together with $|\Delta R_{NL}|$. The linear fits to the data using $\Delta R_{3T} \propto \exp(-d/L)$ are represented as dashed lines. (b) Room-temperature spin-transport length $L(E)$ as a function of E for Si_{0.1}Ge_{0.9} (red) and Ge (black) with $n \sim 1 \times 10^{18} \text{ cm}^{-3}$. The solid curves are simulated data for Si_{0.1}Ge_{0.9} (red) and Ge (black) with $\lambda = 0.93$ and $0.50 \mu\text{m}$, respectively.

in the spin-detection efficiency at a biased Schottky-tunnel contact [66]. These results indicate that the experimentally obtained λ , D , and τ are valid physical quantities for the strained Si_{0.1}Ge_{0.9} with $n \sim 1.0 \times 10^{18} \text{ cm}^{-3}$.

To confirm the effect of electric fields (E) on the long-distance spin transport in the strained Si_{0.1}Ge_{0.9}, we finally examine the exponential decay behavior of ΔR_{3T} with varying d and I_D at room temperature, where the value of I_D is related to that of E in the three-terminal nonlocal measurements in Fig. 4(a). Figure 5(a) shows the d dependence of ΔR_{3T} with varying I_D in a LSV device with the strained Si_{0.1}Ge_{0.9} with $n \sim 1 \times 10^{18} \text{ cm}^{-3}$ at room temperature, together with the d dependence of $|\Delta R_{NL}|$ in the same LSV device. We clearly observe that the exponential decay behavior of ΔR_{3T} becomes evidently moderate when I_D is increased. The dashed lines are linear fits to the data using $\Delta R_{3T} \propto \exp(-d/L)$ at a certain I_D , where L is the spin-transport length. Thus, we can estimate L from the fitting for various E . Figure 5(b) displays plots of L versus E for the strained Si_{0.1}Ge_{0.9} (red) and the pure Ge (black) at room temperature. The estimated L for the strained Si_{0.1}Ge_{0.9} is substantially enhanced with increasing $|E|$ compared to that for the pure Ge.

If E is applied to the spin-transport semiconductor channels, the value of L can become a function of E using the following equation [69–71]:

$$L(E) = \left(\frac{eE}{2\varepsilon_d} + \sqrt{\left(\frac{eE}{2\varepsilon_d} \right)^2 + \left(\frac{1}{\lambda} \right)^2} \right)^{-1}, \quad (3)$$

where e is the elementary charge and $\varepsilon_d (= eD/\mu)$ is an energy scale that controls the strength of the spin drift. Thus, we can simulate L as a function of E using Eq. (3). In the same panel of Fig. 5(b), the calculated $L(E)$ as a function of E using Eq. (3) is depicted, where $\varepsilon_d = 39$ meV and $\lambda = 0.93$ μm for the strained $\text{Si}_{0.1}\text{Ge}_{0.9}$ and $\varepsilon_d = 39$ meV and $\lambda = 0.50$ μm for the Ge are used. Although slight differences between the experimental data and the calculated ones are seen, the strain-induced enhancement in L is roughly reproduced using the enhancement in λ in Eq. (3). Thus, the long-distance spin transport in the strained $n\text{-Si}_{0.1}\text{Ge}_{0.9}$ ($n \sim 1.0 \times 10^{18} \text{ cm}^{-3}$) in Fig. 4 is attributed to the strain-induced enhancement in $L(E)$ at room temperature even in Ge-like conduction-band channels. Therefore, understanding the effect of strain on the spin transport in semiconductors is useful to the development of semiconductor spintronic applications at room temperature.

III. CONCLUSION

The effect of lattice strain on the spin transport in semiconductors is studied using four-terminal nonlocal spin-transport measurements in LSV devices with various semiconductor channels with Ge-like conduction bands. For $n = 1 \times 10^{18} \text{ cm}^{-3}$, the λ of the strained $\text{Si}_{0.1}\text{Ge}_{0.9}$ is much larger than that of the pure Ge at room temperature. A possible mechanism of the strain-induced enhancement of λ is discussed as a consequence of a sufficient energy difference between the conduction valley splitting and E_F at room temperature. Because of the enhancement in λ and L by the strain, 5- μm lateral spin transport at room temperature is electrically detected by applying an electric field to the channel in an LSV device.

ACKNOWLEDGMENTS

This work is supported in part by JSPS KAKENHI (Grants No. 19H05616, No. 19H02175, and No. 21H05000), JST PRESTO (Grant No. JPMJPR20BA), and the Spintronics Research Network of Japan (Spin-RNJ). T.N. acknowledges JSPS Research Fellowship for Young Scientists (Grant No. 21J20019).

-
- [1] F. Cerdeira, C. J. Buchenauer, F. H. Pollak, and M. Cardona, Stress-induced shifts of first-order Raman frequencies of diamond- and zinc-blende-type semiconductors, *Phys. Rev. B* **5**, 580 (1972).
 - [2] O. H. Nielsen and R. M. Martin, Stresses in semiconductors: *Ab initio* calculations on Si, Ge, and GaAs, *Phys. Rev. B* **32**, 3792 (1985).
 - [3] C. G. Van de Walle, Band lineups and deformation potentials in the model-solid theory, *Phys. Rev. B* **39**, 1871 (1989).

- [4] M. V. Fischetti and S. E. Laux, Band structure, deformation potentials, and carrier mobility in strained Si, Ge, and SiGe alloys, *J. Appl. Phys.* **80**, 2234 (1996).
- [5] S. Poncé, D. Jena, and F. Giustino, Hole mobility of strained GaN from first principles, *Phys. Rev. B* **100**, 085204 (2019).
- [6] Q. M. Thai, J. Chretien, M. Bertrand, L. Casiez, A. Chelnokov, V. Reboud, N. Pauc, and V. Calvo, GeSn optical gain and lasing characteristics modelling, *Phys. Rev. B* **102**, 155203 (2020).
- [7] S. Takagi, J. L. Hoyt, J. J. Welser, and J. F. Gibbons, Comparative study of phonon-limited mobility of two-dimensional electrons in strained and unstrained Si metal-oxide-semiconductor field-effect transistors, *J. Appl. Phys.* **80**, 1567 (1996).
- [8] M. L. Lee, E. A. Fitzgerald, M. T. Bulsara, M. T. Currie, and A. Lochtefeld, Strained Si, SiGe, and Ge channels for high-mobility metal-oxide-semiconductor field-effect transistors, *J. Appl. Phys.* **97**, 011101 (2005).
- [9] Y. Sun, S. E. Thompson, and T. Nishida, Physics of strain effects in semiconductors and metal-oxide-semiconductor field-effect transistors, *J. Appl. Phys.* **101**, 104503 (2007).
- [10] T. B. Boykin, M. Luisier, M. Salmani-Jelodar, and G. Klimeck, Strain-induced, off-diagonal, same-atom parameters in empirical tight-binding theory suitable for [110] uniaxial strain applied to a silicon parametrization, *Phys. Rev. B* **81**, 125202 (2010).
- [11] Y. Chuang, C.-Y. Liu, G.-L. Luo, and J.-Y. Li, Electron Mobility Enhancement in GeSn n-Channel MOSFETs by Tensile Strain, *IEEE Electron Device Lett.* **42**, 10 (2021).
- [12] G. C. Osbourn, $\text{In}_x\text{Ga}_{1-x}\text{As}-\text{In}_y\text{Ga}_{1-y}\text{As}$ strained-layer superlattices: A proposal for useful, new electronic materials, *Phys. Rev. B* **27**, 5126 (1983).
- [13] C. Kisielowski, J. Krüger, S. Ruvimov, T. Suski, J. W. Ager, E. Jones, Z. Liliental-Weber, M. Rubin, E. R. Weber, M. D. Bremser, and R. F. Davis, Strain-related phenomena in GaN thin films, *Phys. Rev. B* **54**, 17745 (1996).
- [14] S. Assali, A. Dijkstra, A. Attiaoui, É. Bouthillier, J. E. M. Haverkort, and O. Moutanabbir, Midinfrared Emission and Absorption in Strained and Relaxed Direct-Band-Gap $\text{Ge}_{1-x}\text{Sn}_x$ Semiconductors, *Phys. Rev. Appl.* **15**, 024031 (2021).
- [15] G. Gui, J. Li, and J. Zhong, Band structure engineering of graphene by strain: First-principles calculations, *Phys. Rev. B* **78**, 075435 (2008).
- [16] Z. Gong, X. Shi, J. Li, S. Li, C. He, T. Ouyang, C. Zhang, C. Tang, and J. Zhong, Theoretical prediction of low-energy Stone-Wales graphene with an intrinsic type-III Dirac cone, *Phys. Rev. B* **101**, 155427 (2020).
- [17] W. S. Yun, S. W. Han, S. C. Hong, I. G. Kim, and J. D. Lee, Thickness and strain effects on electronic structures of transition metal dichalcogenides: 2H-MX_2 semiconductors ($M = \text{Mo}, \text{W}$; $X = \text{S}, \text{Se}, \text{Te}$), *Phys. Rev. B* **85**, 033305 (2012).
- [18] O. B. Aslan, M. Deng, M. L. Brongersma, and T. F. Heinz, Strained bilayer WSe_2 with reduced exciton-phonon coupling, *Phys. Rev. B* **101**, 115305 (2020).
- [19] S. Zhang, Z. Yan, Y. Li, Z. Chen, and H. Zeng, Atomically thin arsenene and antimonene: Semimetal-semiconductor and indirect-direct band-gap transitions, *Angew. Chem. Int. Ed.* **54**, 3112 (2015).

- [20] Y. Li, H. B. Zhu, G. Q. Wang, Y. Z. Peng, J. R. Xu, Z. H. Qian, R. Bai, G. H. Zhou, C. Yesilyurt, Z. B. Siu, and M. B. A. Jalil, Strain-controlled valley and spin separation in silicene heterojunctions, *Phys. Rev. B* **97**, 085427 (2018).
- [21] C. Kamal, Massless Dirac fermions in stable two-dimensional carbon-arsenic monolayer, *Phys. Rev. B* **100**, 205404 (2019).
- [22] Y.-J. Yang, W. S. Ho, C.-F. Huang, S. T. Chang, and C. W. Liu, Electron mobility enhancement in strained-germanium n -channel metal-oxide-semiconductor field-effect transistors, *Appl. Phys. Lett.* **91**, 102103 (2007).
- [23] M. Ono and T. Tezuka, Comprehensive study of electron mobility and band gap in tensile-strained bulk Ge, *Jpn. J. Appl. Phys.* **49**, 04DC20 (2010).
- [24] F. Murphy-Armando and S. Fahy, First principles calculation of electron-phonon and alloy scattering in strained SiGe, *J. Appl. Phys.* **110**, 123706 (2011).
- [25] J. Liu, X. Sun, D. Pan, X. Wang, L. C. Kimerling, T. L. Koch, and J. Michel, Tensile-strained, n -type Ge as a gain medium for monolithic laser integration on Si, *Optics Express* **15**, 11272 (2007).
- [26] J. Michel, J. Liu, and L. C. Kimerling, High-performance Ge-on-Si photodetectors, *Nat. Photon.* **4**, 527 (2010).
- [27] F. Bottegoni, G. Isella, S. Cecchi, and F. Ciccacci, Spin polarized photoemission from strained Ge epilayers, *Appl. Phys. Lett.* **98**, 242107 (2011).
- [28] F. Pezzoli, F. Bottegoni, D. Trivedi, F. Ciccacci, A. Giorgioni, P. Li, S. Cecchi, E. Grilli, Y. Song, M. Guzzi, H. Dery, and G. Isella, Optical Spin Injection and Spin Lifetime in Ge Heterostructures, *Phys. Rev. Lett.* **108**, 156603 (2012).
- [29] E. Vitiello, M. Virgilio, A. Giorgioni, J. Frigerio, E. Gatti, S. De Cesari, E. Bonera, E. Grilli, G. Isella, and F. Pezzoli, Spin-dependent direct gap emission in tensile-strained Ge films on Si substrates, *Phys. Rev. B* **92**, 201203(R) (2015).
- [30] N. W. Hendrickx, W. I. L. Lawrie, L. Petit, A. Sammak, G. Scappucci, and M. Veldhorst, A single-hole spin qubit, *Nat. Commun.* **11**, 3478 (2020).
- [31] S. De Cesari, A. Balocchi, E. Vitiello, P. Jahandar, E. Grilli, T. Amand, X. Marie, M. Myronov, and F. Pezzoli, Spin-coherent dynamics and carrier lifetime in strained $\text{Ge}_{1-x}\text{Sn}_x$ semiconductors on silicon, *Phys. Rev. B* **99**, 035202 (2019).
- [32] P. Li and H. Dery, Spin-Orbit Symmetries of Conduction Electrons in Silicon, *Phys. Rev. Lett.* **107**, 107203 (2011).
- [33] J.-M. Tang, B. T. Collins, and M. E. Flatté, Electron spin-phonon interaction symmetries and tunable spin relaxation in silicon and germanium, *Phys. Rev. B* **85**, 045202 (2012).
- [34] Y. Song and H. Dery, Analysis of phonon-induced spin relaxation processes in silicon, *Phys. Rev. B* **86**, 085201 (2012).
- [35] P. Li, Y. Song, and H. Dery, Intrinsic spin lifetime of conduction electrons in germanium, *Phys. Rev. B* **86**, 085202 (2012).
- [36] C. Guite and V. Venkataraman, Temperature dependence of spin lifetime of conduction electrons in bulk germanium, *Appl. Phys. Lett.* **101**, 252404 (2012).
- [37] P. Li, J. Li, L. Qing, H. Dery, and I. Appelbaum, Anisotropy-Driven Spin Relaxation in Germanium, *Phys. Rev. Lett.* **111**, 257204 (2013).
- [38] A. Giorgioni, E. Vitiello, E. Grilli, M. Guzzi, and F. Pezzoli, Valley-dependent spin polarization and long-lived electron spins in germanium, *Appl. Phys. Lett.* **105**, 152404 (2014).
- [39] Y. Song, O. Chalaev, and H. Dery, Donor-Driven Spin Relaxation in Multivalley Semiconductors, *Phys. Rev. Lett.* **113**, 167201 (2014).
- [40] M. Ishikawa, T. Oka, Y. Fujita, H. Sugiyama, Y. Saito, and K. Hamaya, Spin relaxation through lateral spin transport in heavily doped n -type silicon, *Phys. Rev. B* **95**, 115302 (2017).
- [41] M. Yamada, Y. Fujita, M. Tsukahara, S. Yamada, K. Sawano, and K. Hamaya, Large impact of impurity concentration on spin transport in degenerate n -Ge, *Phys. Rev. B* **95**, 161304(R) (2017).
- [42] O. Chalaev, Y. Song, and H. Dery, Suppressing the spin relaxation of electrons in silicon, *Phys. Rev. B* **95**, 035204 (2017).
- [43] T. Naito, M. Yamada, S. Yamada, K. Sawano, and K. Hamaya, Suppression of Donor-Driven Spin Relaxation in Strained $\text{Si}_{0.1}\text{Ge}_{0.9}$, *Phys. Rev. Appl.* **13**, 054025 (2020).
- [44] R. People, Indirect band gap of coherently strained $\text{Ge}_x\text{Si}_{1-x}$ bulk alloys on $\langle 001 \rangle$ silicon substrates, *Phys. Rev. B* **32**, 1405R (1985).
- [45] S. Krishnamurthy, A. Sher, and A.-B. Chen, Band structures of $\text{Si}_x\text{Ge}_{1-x}$ alloys, *Phys. Rev. B* **33**, 1026 (1986).
- [46] K. Sawano, Y. Hoshi, S. Kubo, K. Arimoto, J. Yamanaka, K. Nakagawa, K. Hamaya, M. Miyao, and Y. Shiraki, Structural and electrical properties of Ge(111) films grown on Si(111) substrates and application to Ge(111)-on-Insulator, *Thin Solid Films* **613**, 24 (2016).
- [47] Y. Wagatsuma, M. M. Alam, K. Okada, M. Yamada, K. Hamaya, and K. Sawano, A drastic increase in critical thickness for strained SiGe by growth on mesa-patterned Ge-on-Si, *Appl. Phys. Express* **14**, 025502 (2021).
- [48] K. Hamaya, Y. Fujita, M. Yamada, M. Kawano, S. Yamada, and K. Sawano, Spin transport and relaxation in germanium, *J. Phys. D: Appl. Phys.* **51**, 393001 (2018).
- [49] M. Yamada, T. Ueno, T. Naito, K. Sawano, and K. Hamaya, Experimental extraction of donor-driven spin relaxation in n -type nondegenerate germanium, *Phys. Rev. B* **104**, 115301 (2021).
- [50] J. P. Dismukes, L. Ekstrom, and R. J. Paff, Lattice Parameter and Density in Germanium-Silicon Alloys, *J. Phys. Chem.* **68**, 3021 (1964).
- [51] Q. M. Ma and K. L. Wang, Strain-induced nonlinear energy-band splitting of $\text{Si}_{1-x}\text{Ge}_x$ alloys coherently grown on (111) and (110) oriented Ge substrates, *Appl. Phys. Lett.* **58**, 1184 (1991).
- [52] R. Vrijen, E. Yablonovitch, K. Wang, H. W. Jiang, A. Balandin, V. Roychowdhury, T. Mor, and D. DiVincenzo, Electron-spin-resonance transistors for quantum computing in silicon-germanium heterostructures, *Phys. Rev. A* **62**, 012306 (2000).
- [53] F. J. Jedema, H. B. Heersche, A. T. Filip, J. J. A. Baselmans, and B. J. van Wees, Electrical detection of spin precession in a metallic mesoscopic spin valve, *Nature (London)* **416**, 713 (2002).
- [54] X. Lou, C. Adelmann, S. A. Crooker, E. S. Garlid, J. Zhang, K. S. M. Reddy, S. D. Flexner, C. J. Palmström, and

- P. A. Crowell, Electrical detection of spin transport in lateral ferromagnet-semiconductor devices, *Nat. Phys.* **3**, 197 (2007).
- [55] Y. Fujita, M. Yamada, M. Tsukahara, T. Naito, S. Yamada, K. Sawano, and K. Hamaya, Nonmonotonic bias dependence of local spin accumulation signals in ferromagnet/semiconductor lateral spin-valve devices, *Phys. Rev. B* **100**, 024431 (2019).
- [56] R. Farshchi and M. Ramsteiner, Spin injection from Heusler alloys into semiconductors: A materials perspective, *J. Appl. Phys.* **113**, 191101 (2013).
- [57] M. Jourdan, J. Minár, J. Braun, A. Kronenberg, S. Chadov, B. Balke, A. Gloskovskii, M. Kolbe, H. J. Elmers, G. Schönhense, H. Ebert, C. Felser, and M. Kläui, Direct observation of half-metallicity in the Heusler compound Co_2MnSi , *Nat. Commun.* **5**, 3974 (2014).
- [58] Y. Fujita, M. Yamada, M. Tsukahara, T. Oka, S. Yamada, T. Kanashima, K. Sawano, and K. Hamaya, Spin Transport and Relaxation up to 250 K in Heavily Doped n -Type Ge Detected Using $\text{Co}_2\text{FeAl}_{0.5}\text{Si}_{0.5}$ Electrodes, *Phys. Rev. Appl.* **8**, 014007 (2017).
- [59] M. Yamada, F. Kuroda, M. Tsukahara, S. Yamada, T. Fukushima, K. Sawano, T. Oguchi, and K. Hamaya, Spin injection through energy-band symmetry matching with high spin polarization in atomically controlled ferromagnet/ferromagnet/semiconductor structures, *NPG Asia Mater.* **12**, 47 (2020).
- [60] K. Kudo, M. Yamada, S. Honda, Y. Wagatsuma, S. Yamada, K. Sawano, and K. Hamaya, Room-temperature two-terminal magnetoresistance ratio reaching 0.1% in semiconductor-based lateral devices with $L2_1$ -ordered Co_2MnSi , *Appl. Phys. Lett.* **118**, 162404 (2021).
- [61] M. E. Flatté and J. M. Byers, Spin Diffusion in Semiconductors, *Phys. Rev. Lett.* **84**, 4220 (2000).
- [62] I. Appelbaum, B. Huang, and D. J. Monsma, Electronic measurement and control of spin transport in silicon, *Nature (London)* **447**, 295 (2007).
- [63] B. Huang, D. J. Monsma, and I. Appelbaum, Coherent Spin Transport through a 350 Micron Thick Silicon Wafer, *Phys. Rev. Lett.* **99**, 177209 (2007).
- [64] T. Sasaki, Y. Ando, M. Kamenno, T. Tahara, H. Koike, T. Oikawa, T. Suzuki, and M. Shiraishi, Spin Transport in Nondegenerate Si with a Spin MOSFET Structure at Room Temperature, *Phys. Rev. Appl.* **2**, 034005 (2014).
- [65] S. Sato, M. Tanaka, and R. Nakane, Spin transport in Si-based spin metal-oxide-semiconductor field-effect transistors: Spin drift effect in the inversion channel and spin relaxation in the n^+ -Si source/drain regions, *Phys. Rev. B* **102**, 035305 (2020).
- [66] R. Jansen, A. Spiesser, H. Saito, Y. Fujita, S. Yamada, K. Hamaya, and S. Yuasa, Nonlinear Electrical Spin Conversion in a Biased Ferromagnetic Tunnel Contact, *Phys. Rev. Appl.* **10**, 064050 (2018).
- [67] F. Bottegoni, C. Zucchetti, S. Dal Conte, J. Frigerio, E. Carpene, C. Vergnaud, M. Jamet, G. Isella, F. Ciccacci, G. Cerullo, and M. Finazzi, Spin-Hall Voltage over a Large Length Scale in Bulk Germanium, *Phys. Rev. Lett.* **118**, 167402 (2017).
- [68] C. Zucchetti, F. Bottegoni, C. Vergnaud, F. Ciccacci, G. Isella, L. Ghirardini, M. Celebrano, F. Rortais, A. Ferrari, A. Marty, M. Finazzi, and M. Jamet, Imaging spin diffusion in germanium at room temperature, *Phys. Rev. B* **96**, 014403 (2017).
- [69] Z. G. Yu and M. E. Flatté, Electric-field dependent spin diffusion and spin injection into semiconductors, *Phys. Rev. B* **66**, 201202(R) (2002).
- [70] Z. G. Yu and M. E. Flatté, Spin diffusion and injection in semiconductor structures: Electric field effects, *Phys. Rev. B* **66**, 235302 (2002).
- [71] A. Spiesser, Y. Fujita, H. Saito, S. Yamada, K. Hamaya, W. Mizubayashi, K. Endo, S. Yuasa, and R. Jansen, Quantification of Spin Drift in Devices with a Heavily Doped Si Channel, *Phys. Rev. Appl.* **11**, 044020 (2019).